ChemPhysChem

Research Article
doi.org/10.1002/cphc.202300565

Chemistry Europe
European Chemical Societies Publishing

www.chemphyschem.org

Persistence of Methionine Side Chain Mobility at Low Temperatures in a Nine-Residue Low Complexity Peptide, as Probed by ^{2}H Solid-State NMR

Liliya Vugmeyster,*[a] Dmitry Ostrovsky,[b] Aryana Rodgers,[a] Kirsten Gwin,[a] Serge L. Smirnov,[c] C. James McKnight,[d] and Riqiang Fu[e]

Methionine side chains are flexible entities which play important roles in defining hydrophobic interfaces. We utilize deuterium static solid-state NMR to assess rotameric interconversions and other dynamic modes of the methionine in the context of a nine-residue random-coil peptide (RC9) with the low-complexity sequence GGKGMGFGL. The measurements in the temperature range of 313 to 161 K demonstrate that the rotameric interconversions in the hydrated solid powder state persist to temperatures below 200 K. Removal of solvation significantly reduces the rate of the rotameric motions. We employed ^{2}H NMR line shape analysis, longitudinal and rotation frame relaxation, and chemical exchange saturation transfer methods and found that the combination of multiple techniques creates a significantly more refined model in comparison with a single technique. Further, we compare the most essential features of the dynamics in RC9 to two different methionine-containing systems, characterized previously. Namely, the M35 of hydrated amyloid-β_{1-40} in the three-fold symmetric polymorph as well as Fluorenylmethyloxycarbonyl (FMOC)-methionine amino acid with the bulky hydrophobic group. The comparison suggests that the driving force for the enhanced methionine side chain mobility in RC9 is the thermodynamic factor stemming from distributions of rotameric populations, rather than the increase in the rate constant.

Introduction

Methionine side chains are rather unique, as they are the only non-branched, non-aromatic hydrophobic side chains with a high degree of mobility found often in hydrophobic cores and interfaces.[1–14] Their structure and dynamics are often important in defining the properties of such interfaces and subsequent ligand binding properties.[11,15] Their flexibility is often needed for an overall structural plasticity of hydrophobic interfaces.[11,13,16] Methionine has three dihedral angles (χ_1, χ_2, χ_3), which, in principle, permit 27 possible rotamers (Figure 1A). Depending on the spatial restriction caused by molecular environment, usually only a few of these rotamers would be populated.[17] Relative populations of these rotamers and interconversions between them could define functionality.[4,18]

We previously utilized ^{2}H solid-state NMR to investigate the dynamics of a methionine in amyloid-β (Aβ_{1-40}) fibril systems[5–6] and in the fluorenylmethyloxycarbonyl (FMOC)-methionine amino acid.[7] The bulky FMOC group defines intra and intermolecular packing and somewhat mimics the environment found in the hydrophobic cores.[7,19] A significantly more diverse and heterogenous hydrophobic core environment in proteins due to the presence of multiple functional groups provides a limitation to the extent of this analogy.

With the use of various ^{2}H NMR techniques, such as line shape,[5,20–23] laboratory frame relaxation,[20,24] rotating frame relaxation,[25–26] and quadrupolar chemical exchange saturation transfer (Q-CEST) measurements,[27–28] it is possible to obtain both the relative rotameric populations within the chosen model and the rate of interconversions of the rotamers. FMOC-methionine amino acid in the dry state displayed a considerably more rigid behavior in comparison to the M35 in Aβ_{1-40} fibrils. The dynamics in the latter[5–6] appears to be defined by the water accessible cavity[3,29] between the fibrillar subunits in the 3-fold symmetric structure,[30–31] to which the methionine side chain points.

In this work we utilize a nine-residue peptide construct with a low complexity[32–33] primary sequence. The sequence is GGKGMGFGL, to which we introduce a single-site deuterium label at the methyl group of M5. We referrer to this peptide as "RC9", in which "RC" stands for the random coil. The construct is a useful model system (or a monomeric unit) for studies of naturally occurring low complexity disordered proteins, such as those involved in phase separation phenomenon.[33] Here, we

[a] L. Vugmeyster, A. Rodgers, K. Gwin
Department of Chemistry, University of Colorado Denver, 1201 Larimer St, Denver CO USA 80204
E-mail: liliya.vugmeyster@ucdenver.edu

[b] D. Ostrovsky
Department of Mathematics, University of Colorado Denver, 1201 Larimer St Denver CO USA 80204

[c] S. L. Smirnov
Department of Chemistry, Western Washington University, 516 High Street, Bellingham, WA 98225

[d] C. J. McKnight
Department of Pharmacology, Physiology and Biophysics, Boston University Chobanian and Avedisian School of Medicine, 72 E Concord Street, Boston, MA, 02118

[e] R. Fu
National High Magnetic Field Laboratory, 1800 E Paul Dirac Drive, Tallahassee, FL USA 32310

Supporting information for this article is available on the WWW under https://doi.org/10.1002/cphc.202300565

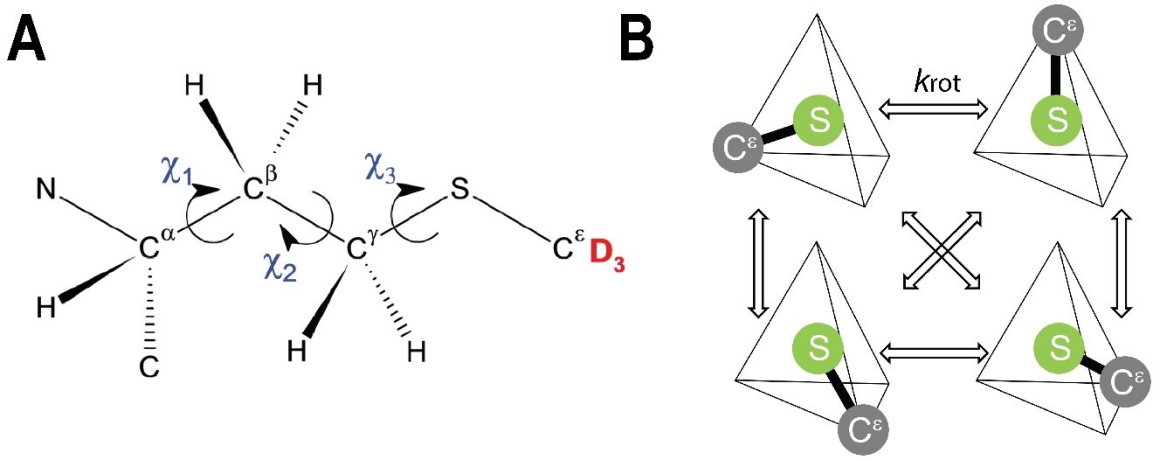

Figure 1. A) The structure of methionine amino acid with the position of deuterium label indicated in red and an explicit notation for the three side chain dihedral angles. B) The motional model involving rotameric jumps between four magnetically inequivalent positions of the S–C$^{\varepsilon}$, under the assumption of the ideal tetrahedral geometry in all 27 real methionine rotamers.

investigate the details of its M5 side chain dynamics in the solid powder state with and without the hydration layer. Its dominant feature is the persistence of rotameric interconversions to remarkably low temperatures below 200 K.

Many studies of proteins in the solid-state are performed for hydrated powders or gel-like phases, including the extensively studied amyloid-β, α-synuclein and tau fibrils and oligomers.[30,34–35] Most neutron scattering studies of hydrated globular proteins that probe dynamical transitions are also employing hydrated powder states.[36–39] Taken together, the three systems that we consider in this work permit for examining dynamic properties of methionine side-chains in more detail. The conclusions of this work are not confined to powder-like solid samples, as they depend on micro-environment around the methyl side-chains. For example, the microcrystalline protein state, which is often employed in solid-state NMR measurements for site-resolved resolution,[40] is expected to behave similarly in this respect.

Results and Discussion

Selected structural assessment.

We have not assessed the entire structure of the RC9 peptide in the solid state but have instead focused on determining the ^{13}C chemical shift at the methyl carbon of the M5, as it provides a sensitive probe of rotameric populations around the χ_3 dihedral angle.[12] In particular, we used proton to carbon cross-polarization spectrum at 60 kHz magic angle spinning conditions (Figure S1). For this measurement we used the peptide that had both a ^{13}C and deuterium labels at the methionine methyl group and the peptide was in the dry powder state. The carbon chemical shift for the methyl group was found to be 16.2 ± 0.2 ppm. This value implies the predominance of the *gauche* conformation for the χ_3 dihedral angle, but also a significant population of the *trans* rotamer, with the two rotamers undergoing conformational exchange on the chemical shift time scale.[12]

We also characterized the structural properties of the entire peptide in solution, described in detail in SI1. The peptide shows a random-coil structure based on conventional backbone amide proton NMR resonance assignments[41] (Figures S2,S3 and Table S1) and circular dichroism measurements (Figure S4). The ^{13}C chemical shift of the methionine methyl group in solution is 16.6 ppm. The value of 16.6 ppm is within the average value of 17.1 ppm reported for methionine methyl groups, with the standard deviation of 1.7 ppm.[42–43] There is a good agreement between the solid and solution state values of this chemical shift. The solution NMR backbone and selected side chain assignments have been deposited to BMRB data bank with the ID 51754.

Combined analysis of ^{2}H NMR static line shape and rotating frame relaxation rates

Our main tools to investigate rotameric interconversions in methionine are the deuterium line shape measurements as well as rotating frame relaxation rate measurements ($R_{1\rho}$) under static conditions, which are both sensitive to motions on μs to ms time scales.[28,44–45] In order to define the kinetic and thermodynamic variables of the system, it is desirable to cover a broad temperature range, so that one can obtain accurate activation energies of rotameric interconversions as well as changes in the distributions of the rotameric populations.

We first present the results for the hydrated RC9 peptide at pH 2, whose hydration state of 80 % by weight was achieved by the incorporation of deuterium depleted water, as described in the "Materials and Methods" section. The line shapes (Figure 2) were taken in the 313 to 161 K temperature range, while $R_{1\rho}$ rates were determined from 313 K to 242 K (Figure 3). The $R_{1\rho}$ rate measurements are significantly more challenging from the

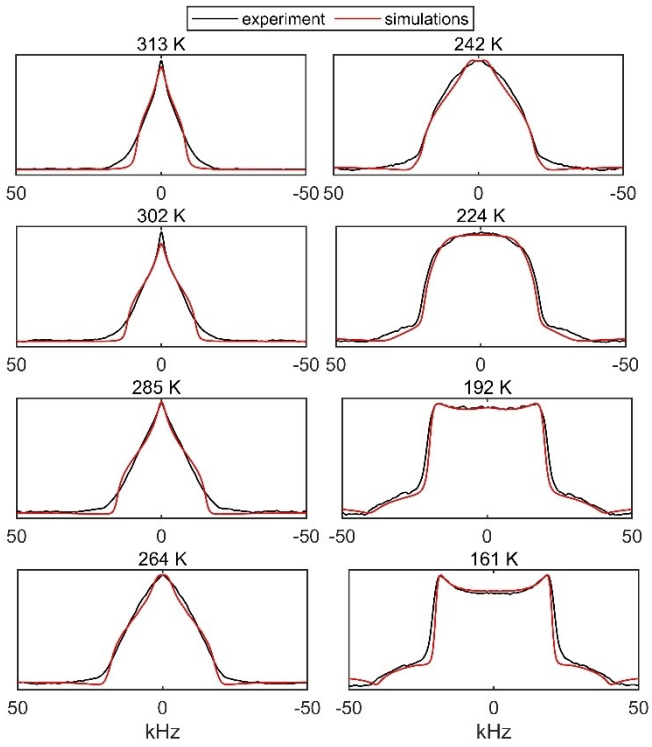

Figure 2. Examples of experimental (black) and modeled (red) ^{2}H static solid-state NMR line shapes in M5-CD_3 side chain of the hydrated RC9 peptide at pH 2 and 80% hydration level, collected at 9.4 T with the quadrupolar echo pulse sequence. The fits were performed according to the rotameric exchange model of Figure 1B with $w_2 = w_1$ for high temperatures and $w_1 > w_2$ for lower temperatures below 264 K, as described in the text.

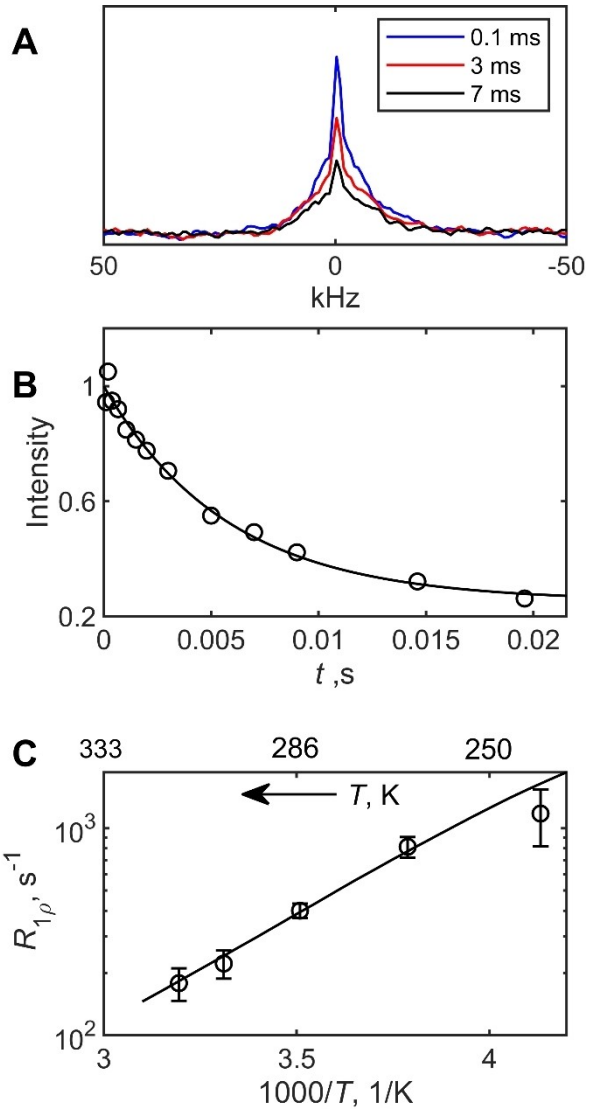

Figure 3. Results for the on-resonance ^{2}H NMR $R_{1\rho}$ measurements for the M5-CD_3 side chain of RC9 in the hydrated powder state at 9.4 T and employing the spin-locking field of 20 kHz field strength. A) Examples of partially decay spectra for different relaxation delay times for the measurements at 313 K and B) The corresponding normalized magnetization decay curve, intensity versus time. The line represents the fit to the mono-exponential function with a baseline. C) The on-resonance ^{2}H $R_{1\rho}$ relaxation rates versus 1000/*T*. The upper *x*-axis shows the direct temperature scale. The line represents the fit to the 4-rotamer exchange model of Figure 1B, as described in the text.

technical standpoint, and we found the narrower temperature range sufficient to characterize the rotameric motions.

The on-resonance $R_{1\rho}$ measurements rely on the application of the spin-locking field for a variable duration to obtain the decay of magnetization in the rotating frame (Figure 3A, B). The RF field of 20 kHz was chosen for the on-resonance measurements, which ensures sufficient spin-locking of the magnetization without excessive RF-induced heating effects.[25] The magnetization decay curves (Figure 3B) are fitted to the mono-exponential function with a baseline. The resulting $R_{1\rho}$ rates are shown in Figure 3C as a function of the inverse temperature. The dependence is approximately linear, indicating Arrhenius behavior.

Under the assumption of the ideal tetrahedral sp^3 bond geometry, for all 27 real methionine rotamers there are four magnetically inequivalent orientations of the S–C$^\varepsilon$ axis in the molecular frame. These inequivalent orientations point toward the corners of the tetrahedron.[5] The combined effect of rotations about side chain dihedral angles to yield magnetically inequivalent conformers with the tetrahedral geometry has been previously described in the literature.[24,46–47] While in reality there are deviations from the tetrahedral geometry in methionine,[12,48] the use of this assumption allows for simplification of the complexity of the rotameric space and we adopt this assumption in our simulations. Under this assumption, we introduce the model which consists of jumps between four positions of the S–C$^\varepsilon$ axis, demonstrated in Figure 1B, without the direct connection to the side chain dihedral angles. The full break-down of the 27 conformers into the space of these four magnetically inequivalent S–C$^\varepsilon$ axis orientations is given in Table S2, along with the most likely to be populated based on the backbone-dependent rotameric library of Shapovalov and Dunbrack.[48] The population of these conformers are dependent on local packing densities around the side-chains, steric effects, water exposure, and other factors influencing the complexity of protein environment.

For the four-state S–C$^\varepsilon$ axis model, the simplest assumption is to have one major conformer with the relative weight of *w*

and three minor conformers with equal weights, such as their relative ratios are defined by w:1:1:1. The rate of rotameric interconversions (k_{rot}) is assumed to be the same between all four rotamers, as the simplest assumption. We then can conduct a joint fit of the line shape and $R_{1\rho}$ data. Using this approach, the temperature-dependent values of w can be reconciled between the two data sets, however the rotameric rate constants are different by orders of magnitude (Figure 4A).

This conclusion is reminiscent of what we previously observed for the FMOC-methionine and M35 side chain of Aβ fibrils, which required different assumptions to fit both the line shape and $R_{1\rho}$ or Q-CEST data simultaneously.[26–27] In particular, we had to assume two major conformers and two minor ones. Following a similar logic, we now move to the modified population ratios of w_1:w_2:1:1. The simplest case is given by $w_1 = w_2$ for all temperatures. The $R_{1\rho}$ rates are relatively insensitive to changes in the distribution of the rotameric populations and depend primarily on the value of k_{rot}, while the line shapes in this range are very sensitive to the rotameric populations. The separation of the sensitivities of these two experiments to the rotameric populations and the rate constant is due to the fact that at high temperatures the rotameric rates required to fit the $R_{1\rho}$ experiments are already close to the fast motional limit for the line shapes, i.e., $k_{rot} \gg C_q$, in which C_q is the value of the quadrupolar coupling constant.

This assumption holds down to about a temperature of 264 K, with the fitted values of temperature-dependent weights, $w_1 = w_2$, in the 2.5 to 18 range (Figure 4C, D). The values of k_{rot}, which fit both the line shape and $R_{1\rho}$ data, follow the Arrhenius behavior $k_{rot}(T) = k_0 e^{-E_a/RT}$ with the activation energy E_a of 26 ± 2 kJ/mol and the prefactor k_0 of 2–6·10^{11} s^{-1}.

However, starting at the temperature of about 264 K and becoming even more pronounced for lower temperatures in the 242–220 K range, the line shapes simulated with this model (Figure S5) display a symmetric peak at zero frequency, which is absent in the experimental data. This indicates that the symmetry of the rotameric population distributions breaks down further at lower temperatures and we have to proceed to the model with $w_1 > w_2$. To be consistent throughout the whole temperature range we keep the sum $w_1 + w_2$ at each temperature the same, as it would be for the case for $w_1 = w_2$. We, thus, apply this more involved model in the 264 to 161 K temperature range, and the simulated results of Figure 4B, C show the fits incorporating the $w_1 > w_2$ assumption. Below about 264–242 K the contributions from the other two minor conformers, while included in the simulations, are extremely minor (below 2% at 242 K) and we are effectively in the regime of two remaining rotamers. The values of k_{rot} below 242 K were taken by projecting the Arrhenius temperature dependence of the rate constant obtained on the basis of the $R_{1\rho}$ measurements. As stated above, the line shape simulations in this motional regime are not very sensitive to the exact value of the rate constant, and therefore the uncertainties inherent in this projection have a minor effect on the fitted values of the weights. The relative ratio of w_1/w_2 is shown in Figure 4D, which

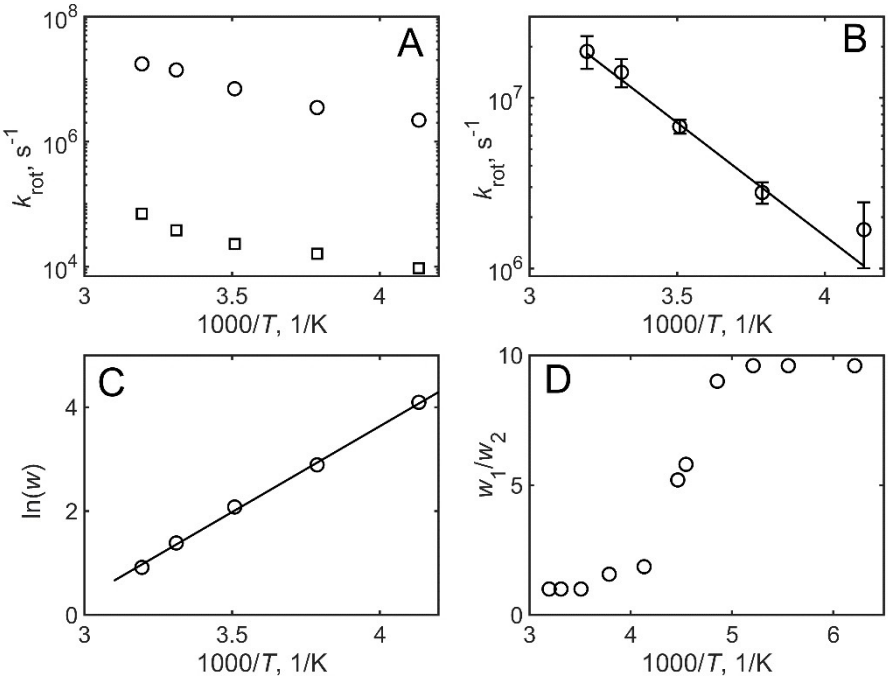

Figure 4. The parameters of the model: A) A semi-log plot of the fitted values of k_{rot} versus 1000/T, obtained individually either on the basis of the ^{2}H NMR line shapes (squares) or the on-resonance ^{2}H NMR $R_{1\rho}$ rates (circles) using the model of Figure 1B and the assumption of rotameric populations in the w:1:1:1 ratio. B) k_{rot} versus 1000/T from the joint fit of the $R_{1\rho}$ and line shape data using the w_1: w_2:1:1 assumption for the rotameric populations with $w_1 = w_2 = w$ and C) the corresponding plot of ln$w$ versus 1000/T. The lines represent the linear fit to the temperature dependence with the Arrhenius activation energy of rotameric motions of 26 ± 2 kJ/mol. The fitted values of the energy difference between the major and minor rotameric states is 28 ± 2 kJ kJ/mol. D) The ratio of rotameric populations, w_1/w_2 versus 1000/T, using the w_1:w_2:1:1 model of Figure 1B across the entire temperature range of 313 to 161 K based on the joint fit of line shape and $R_{1\rho}$ data.

has a distinct sigmoidal shape, indicating that by 200 K a single rotameric state predominates.

Thus, the joint analysis of the ^{2}H NMR line shape and $R_{1\rho}$ rates is a powerful combination for obtaining the details of relative weights of the rotamers. However, from the structural perspective we do not know to which dihedral angles (χ_1, χ_2, χ_3) these rotameric states correspond to.

Additional experiments in support and refinement of the model: laboratory frame T_1, off-resonance $R_{1\rho}^{off}$, Q-CEST

Additional dynamics experiments that can be sensitive to rotameric interconversions include off-resonance rotating frame relaxation rate ($R_{1\rho}^{off}$) measurements and quadrupolar CEST under static conditions.[26–27] Additionally, at high temperatures laboratory frame T_1 relaxation is expected to probe these motions as well when they dominate over the 3-site methyl jumps around S–C$^\gamma$ axis.[6] The 3-site methyl jumps are often referred in the literature by the term "methyl rotations."[49]

The deuterium $R_{1\rho}^{off}$ and Q-CEST[27] measurements were conducted at the highest temperature of 313 K (Figure 5). The $R_{1\rho}^{off}$ experiments are similar in nature to the on-resonance case, except that the spin-locking field is applied off-resonance. In these experiments, the magnetization is spin-locked along the tilted frame and the range of effective spin-locking field can be increased without the increase in the RF-induced heating: the effective field ω_{eff} is given by the vector sum of ω_{RF} (the spin-lock field) and Ω (the off-resonance offset). The alignment of the quadrupolar order along the tilted axis is accomplished by the use of adiabatic shape pulses, optimized for deuterium as described in our prior work.[26] For these measurements we used the value of ω_{RF} of 30 kHz, and the range of offsets from 5 to 75 kHz. The optional inversion pulse was used before the alignment to enhance the precision of the measurements.[26] An example of a magnetization decay curve is shown in Figure S6 and the resulting dispersion profile is demonstrated in Figure 5A. The prediction of the model used above with the parameters determined from the on-resonance $R_{1\rho}$ and line shape measurements (i.e, the weights in the 2.5:2.5:1:1 ratio and the rotameric exchange constant of $1.9\cdot10^7$ s^{-1}) is in excellent agreement with the experimental data.

In the deuterium Q-CEST measurements (Figure 5B) a weak RF field, 1.6 kHz in our case, is applied to the equilibrium magnetization as a function of the off-resonance offset. The presence of the dynamics causes the characteristic loss of intensity for the offsets matching the orientation-dependent frequencies of the quadrupolar interaction.[27] The saturation time was set to 20 ms, which is much shorter than the longitudinal relaxation time of 180 ms determined at this temperature. The Q-CEST experiment is complementary in nature to both the on-resonance and the off-resonance $R_{1\rho}$ measurements. The saturation profile can be matched well with the ratio of weights given by 2.5:2.5:1:1 and a slightly lower k_{rot} of $1.7\cdot10^7$ s^{-1}. Thus, these additional measurements confirm the applicability of the rotameric inter-conversion model and its fitted parameters.

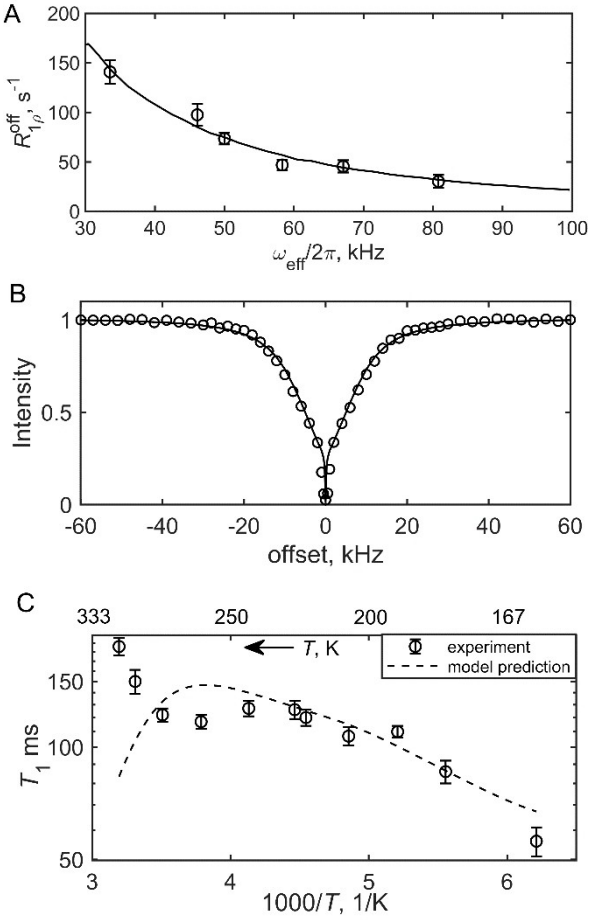

Figure 5. A) ^{2}H solid-state NMR $R_{1\rho}^{off}$ relaxation rates versus effective field strengths for the spin-locking field of 30 kHz in the hydrated side chain of M5-CD$_3$ of RC9 at 313 K and 9.4 T and B) Q-CEST results at the same conditions. Normalized intensity versus offset, obtained using the saturating field strength of 1.6 kHz and the saturation time of 20 ms. The solid lines represent the fit according to the model of Figure 1B with the relative weights of rotamers given by 2.5:2.5:1:1 and k_{rot} of $1.9\cdot10^7$ s^{-1}. C) ^{2}H NMR T_1 relaxation times, on the semilog scale, versus 1000/T. The upper x-axis shows the direct temperature scale. The dotted line represents the fit to the two-mode model of 3-site jumps and rotameric interconversions, as detailed in the text.

The situation becomes more complex when we consider laboratory frame relaxation, performed in the 313 to 161 K temperature range. Motions on the order of ^{2}H Larmor frequency (which is 61 MHz in our case) are most effective in causing relaxation. In the measured T_1 relaxation times (Figure 5C and Figure S7), there appear to be at least two inflections as a function of temperature. T_1 decreases from 333 to 270 K, then levels out, until about 220 K where it begins to decrease again. At the lowest temperatures (i.e., the 220 to 161 K region) the motions of fast methyl 3-site jumps rather than rotameric interconversions are most effective in causing relaxation, while at higher temperatures we have a competition between these methyl jumps, rotameric inter-conversions, and potentially intra-well motions within the rotameric wells.[6–7] The log(T_1) trend in the low temperature range from 224 K to 161 K is approximately linear as a function of the inverse temperature, and we, therefore, assume that they are dominated by the 3-

site methyl jumps. A moderate extent of non-exponentiality was observed only at the lowest temperature point, and, thus, the whole temperature range was fitted with a single-exponential magnetization build-up function. The methyl 3-site jumps mode in the 224 K to 161 K can be fitted the activation energy of 3.0 kJ/mol and the Arrhenius prefactor of $7 \cdot 10^{10}$ s^{-1}. The next step is to include the rotameric motions with the weights and rotameric inter-conversion rate constants as determined from the line shape and on-resonance $R_{1\rho}$ measurements. With the inclusion of these rotameric inter-conversions and the 3-site jumps modes, the results are given by dashed line in Figure 5C. There is considerable disagreement present at the two highest temperatures. The model underestimates T_1 times in this regime. One of the likely explanations for this deviation is the presence of intra-well motions on the time scale similar to the time scale of the rotameric inter-conversions. These intra-well motions appeared to be dominant at high tempeatures in other hydrated methionine side chains, such as the M35 site in Aβ fibrils.[6] If they occur on similar time scales as the large angle rotameric jumps, it is difficult to model them accurately, but they can be intuitively expected to lower the relaxation rates due to effective decrease in individual jump angles from one rotameric well to another in the presence of the large amplitude of motions inside the well.

As the $R_{1\rho}^{off}$ and Q-CEST experiments are performed off-resonance and can have a significant longitudinal relaxation component, their explicit modeling requires an accurate inclusion of mechanisms responsible for longitudinal relaxation rates. Because the methyl 3-site jumps are an inefficient mechanism of relaxation at high temperatures, and the rotameric jumps by themselves already yield the value of the relaxation rate which is higher than experimental one, we did not include any modes other than rotameric jumps in the modeling procedures.

Effect of hydration on the rotameric motions of RC9

Solvation of proteins is known to enhance dynamics, even for sites that are not in direct contact with water.[39,50] Our prior work also indicates that the hydration of methyl bearing side chains can enhance rotameric inter-conversions and intra-well motions in protein and amyloid fibrils.[5,51–52]

The dynamics of the methionine side chain of the unstructured RC9 peptide are also strongly dependent on the solvation. Figure 6A compares the spectra in the dry and the 80% solvated states at 313 K and 242 K. The dry state has a wider pattern indicative of the substantial suppression of the rotameric motions across the wide temperature range. Additionally, the $R_{1\rho}^{off}$ rates are higher in the dry states (Figure 6B). Note we are in the so-called fast regime as follows from Figure 3C, in which $R_{1\rho}$ is inversely proportional to k_{rot}.[53] Thus, the larger value of $R_{1\rho}^{off}$ in the dry state signifies a decrease in the rotameric exchange rate constant in comparison to the wet state.

Comparison with methionine methyl groups in Aβ fibrils and FMOC-methionine

To place the results of the methionine side chain of RC9 in a broader context we compare it to the methionine in $A\beta_{1-40}$ fibrils and to FMOC-methionine. Specifically we compare the hydrated RC9 dynamics to hydrated $A\beta_{1-40}$ fibrils in the 3-fold symmetric polymorph, and the FMOC-methionine dry amino acid.[6–7,27] The side chain of M35 in the $A\beta_{1-40}$ fibrils is believed to point into the interface between different subunits of $A\beta_{1-40}$ and its dynamics can differ depending on the polymorphic state, mutations, or post-translational modifications.[54] In the 3-fold symmetric polymorph[30–31] it is pointed into a water accessible cavity.[3,29] As mentioned in the introduction, the bulky FMOC group of the FMOC-methionine amino acid (Figure S8) partially mimics the environment found in the hydrophobic cores.[7,19]

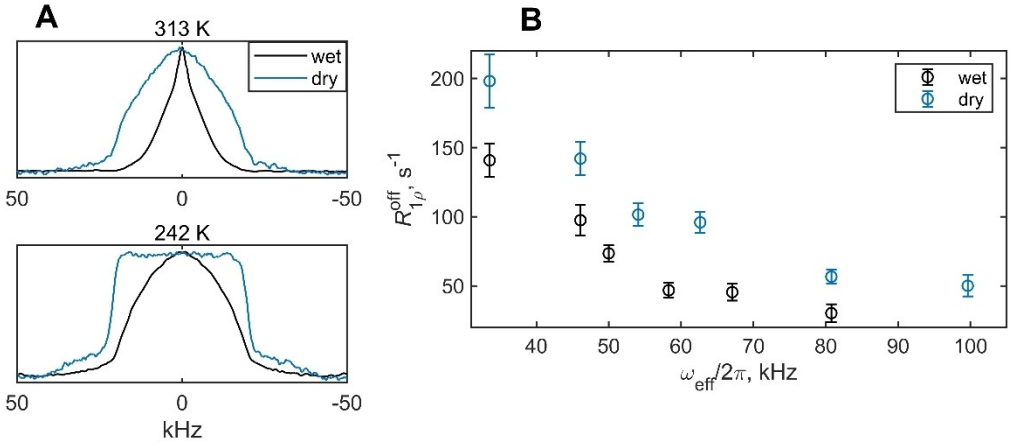

Figure 6. Comparison of A) ^{2}H solid-state NMR line shapes at 313 K and 242 K and B) ^{2}H NMR $R_{1\rho}^{off}$ relaxation rates as function of effective field at 313 K and 9.4 T for the hydrated (80% by weight) and dry states of the M5-CD_3 side chain in RC9.

The ^{2}H solid-state NMR line shape narrowing due to motions displays the following order: RC9 is the most narrowed, followed by the Aβ fibrils, and then by the amino acid (Figure 7A). Figure 7B displays a qualitative comparison of T_1 values as a function of temperature. At the lower temperature end for all systems, T_1 relaxation times are dominated by the 3-site methyl jumps. At the high end of the temperature range, rotameric interconversions and/or intra-well fluctuations dominate the dynamics of the hydrated Aβ fibrils and the hydrated RC9 peptide. The change in the dominance of the relaxation mechanism is referred to as the dynamical crossover[6,50,55] and it manifested in the change in the slope in the Arrhenius-type plots of lnT_1 versus the inverse temperature (Figure 5C and S9). We observe that for RC9 the flatter portion of the curve, signifying the dominance of the methyl axis motions, persists to significantly lower temperature of about 192 K, in comparison to the other two systems (Figure 5B). In the dry FMOC-methionine the dynamical cross-over is absent and the T_1 relaxation is defined primarily by the 3-site methyl jumps at all temperatures. In the M35 side chain of the Aβ fibrils in the hydrated state, the cross-over is clearly visible at around 250 K. In the case of the dry fibrils the cross-over is practically quenched.[6] Thus, the onset temperature of large-scale rotameric fluctuations appears to be correlated with the overall hydrophobicity of the environment around the side chain. Thus, hydration enhances rotomeric interconversion. It is possible that the stable hydrophobic cavities in the FMOC-methionine amino acid and the 3-fold symmetric Aβ_{1-40} fibrils' raise the onset temperature of rotameric fluctuations.

Figures 7C and 7D display the values of w_1, w_2 and k_{rot} obtained with the model of Figure 1B for the three systems based on the line shapes and/or $R_{1\rho}$ and Q-CEST measurements at 37 ± 3 °C. FMOC-methionine has a larger value of $w_2 + w_1$ (i.e., relative weights of the two major conformers) as well as non-equal weights of the two conformers, while in the fibrils and RC9 the weights of the two major conformers are equal and the values are smaller. In particular, in RC9 $w_2 = w_1 = 2.5$, in the Aβ_{1-40} fibrils $w_2 = w_1 = 6$, and in FMOC-methionine $w_1 = 13$, $w_2 = 6$. In contrast, the values of k_{rot} are comparable in FMOC-methionine and RC9, but it is almost an order of magnitude smaller in the Aβ_{1-40} fibrils (Figure 4D). If the overall qualitative extent of mobility is defined by the observed line shape narrowing and the dynamical cross-over in the T_1 curve, we conclude that the driving factor in the mobility changes in these three cases is thermodynamic in nature. In particular, in the disordered hydrated RC9 peptide the populations of the rotameric states are most equalized.

Lee at al.[15] have shown that temperature-dependence of methyl axes order parameters in calmodulin can be compared with the temperature dependence of the average mean squared atomic displacements obtained from neutron scattering studies of proteins.[56–59] They use this observation to conclude that the onset of rotameric jumps can be, at least partially, responsible for the glassy transition related to the

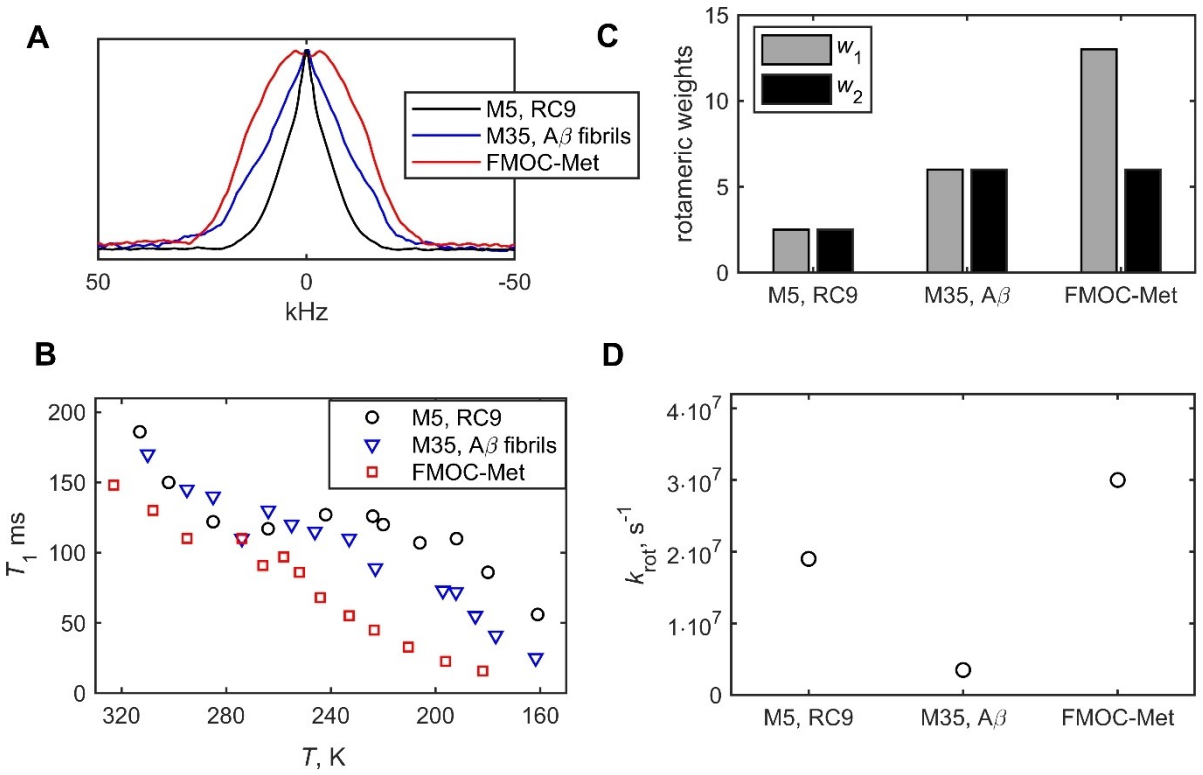

Figure 7. Comparison between different methionine-bearing systems: M5 in hydrated RC9, M35 in Aβ_{1-40} fibrils in the hydrated 3-fold symmetric polymorph, and dry FMOC-methionine amino acid.[6–7,26–27] A) ^{2}H solid-state NMR line shapes at around 37 °C and 9.4 T. B) ^{2}H NMR T_1 times versus T at 9.4 T. Rotameric populations (C) and k_{rot} (D), obtained on the basis of the line shapes, $R_{1\rho}$ rates, as well as Q-CEST experiments at around 37 °C and fitted according to the model of Figure 1B.

onset of slow motions important in events such as ligand binding, protein interactions and enzymatic catalysis.[36,39,59–61] The methyl axes order parameters reflect the extent of methyl axes motions, which include rotameric inter-conversions and intra-well fluctuations. Thus, the role of the distribution of the rotameric populations in the increased mobility of the methionine side chain in the RC9 peptide and its persistence at low temperature is in line with the studies of Lee et al.

Most prior studies of the dynamical cross-overs and the effect of hydration on such have been performed on larger protein systems. It is thus interesting to observe that the dynamical cross-over from the dominance of methyl rotations at low temperatures to the dominance of rotameric interconversions at high temperatures is very pronounced in this short low-complexity peptide. Lewandowski et al.[61] used solid-state NMR relaxation techniques over at a wide-temperature range to determine the hierarchical features of internal dynamics in hydrated crystalline GB1 protein. In particular, they suggested that the onset of large scale fluctuations of side chains occurs in the 220 to 250 K temperature range. Results from multiple neutron scattering studies of globular proteins in the hydrated powder state also indicate that in this temperature range one observes a pronounced activation of solvent-coupled modes and, especially, those of side-chains (as summarized in[36–39] and the references within). Our results for the Aβ fibrils are in line with this determined range, while the short disordered RC9 peptide displays a lower temperature of around 190 K. It is interesting to note that according to the simulations of Figure 4D, at 190 K a single rotameric state is dominant, with a sharp sigmoidal onset of additional states at higher temperatures. It is possible that the persistent of methyl axis fluctuations of methionine side chains in hydrated disordered low complexity systems can be a functional feature not only for this short peptide, but for naturally occurring polypeptide sequences and disordered low complexity domains of proteins involved in multiple cell functions, including liquid-liquid phase separation.[32–33]

Conclusions

Using the combination of ^{2}H solid-state NMR line shape analysis and rotating frame relaxation measurements, we demonstrated that the rotameric interconversions of the M5 side chain persists to temperatures below 200 K in the RC9 peptide in the hydrated powder state. The rotameric inter-conversions are significantly diminished in the dry state of the peptide. The model of jumps between four magnetically inequivalent positions with tetrahedral geometry was employed to fit the experimental data. This model is applicable across the entire temperature range of 313 to 161 K to approximate rotameric inter-conversions in methionine. The relative ratio of these artificial rotameric populations changed dramatically over this temperature range. At the highest temperature the ratio was 2.5:2.5:1:1, representing two equally populated major conformers. At the intermediate temperature range of 264 to 225 K the populations of the major conformers became non-equivalent while the populations of minor rotamers became negligible. Finally, at the lower temperature range the populations of the two major rotamers converged to the essentially single state by 200 K. This transition occurred in the sigmoidal fashion as a function of inverse temperature. This detailed picture of the rotameric populations could not be obtained on the basis of either the line shape or $R_{1\rho}$ measurement alone, as each of them independently could be fitted within the *w*:1:1:1 model, albeit with very different rotameric rate constants. It is interesting that both the $R_{1\rho}^{off}$ and Q-CEST measurements entirely corroborated the model and the corresponding fitted parameters. In contrast, the T_1 relaxation times, which are sensitive to motions on the order of Larmor frequency, showed that the methyl axis also participates in the intra-well motions at high temperatures, which are similar in their time scale to the rotameric jumps.

The comparison with the side chain of M35 in the 3-fold symmetric hydrated $A\beta_{1-40}$ fibrils and FMOC-methionine amino acid highlighted the persistence of rotameric interconversions and intra-well motions in RC9 to very low temperatures. It is interesting to observe that the dynamical cross-over from the dominance of methyl rotations at low temperatures to the dominance of rotameric inter-conversions at high temperatures is very pronounced in this short low-complexity peptide, as most prior investigations have focused on the dynamical cross-overs in larger protein systems. The observed transition temperature in the hydrated RC9 peptide is approximately 190 K, which is the lowest among the three systems.

Further, the comparison of the fitted parameters of rotameric populations and rate constants based on the line shapes and $R_{1\rho}$/Q-CEST measurements for these three systems at the physiological temperature implies that the persistence of the methyl axis dynamics in the M5 side chain of RC9 is caused by different distributions of rotameric populations. In particular, in the hydrated RC9 peptide the populations of the rotameric states are most equalized compared to the other two systems, while its rotameric exchange rate constant is similar to that of FMOC-methionine. The results highlight the physical basis of how methionine side chains can retain their functional mobility in low complexity systems. The mobility of methionine side chains in low complexity systems may turn out to be an essential function in protein-protein interactions, especially at hydrophobic interfaces.

Materials and Methods

Peptide preparation

The RC9 peptide with the sequence GGKGMGFGL was prepared using solid-state peptide synthesis using the FMOC-based chemistry by Life Technologies, Inc and purified by reversed-phase high pressure liquid chromatography(HPLC) using the C18 column and the water/acetonitrile gradient with trifluoroacetic acid as the co-factor. The purity of the peptide at 98% level was confirmed by analytical HPLC (0.5% acetonitrile/min gradient), matrix-assisted laser desorption/ionization mass spec-

troscopy, and proton solution NMR. The peptide used in the main text had a -CD_3 label at the M5 position. FMOC-Met-D_3 amino acid was purchased from Cambridge Isotope laboratories. Additional labeling patterns for spectra in the structural studies presented in the Supporting Information are mentioned in the SI figure legends and text.

The peptide was dissolved in millipore-filtered water and the pH was adjusted to 2, proceeded by lyophilization. For the static deuterium solid-state NMR measurements, 11 mg of dry peptide was packed into a 5 mm glass tube. The hydrated state corresponded to the direct addition of 8.7 μl deuterium depleted water (purchased from Cambridge Isotopes laboratories). The water was mixed in and the sample frozen, thawed, and equilibrated for 48 hours at room temperature to achieve a homogeneously hydrated state.

NMR spectroscopy

Static solids-state ^{2}H NMR measurements were conducted using the 9.4 T spectrometer at CU Denver equipped with the static Phoenix probe with the 5 mm diameter coil. Line shape measurements were measured using the quadrupolar echo (QE) pulse sequence involving an 8-step phase cycle[20] with the echo delay of 35 μs. The inter-scan delay was set to at least a factor of three times larger than the longitudinal relaxation times. The number of scans varied between 10,240 and 2,560. Laboratory frame longitudinal relaxation measurements employed saturation recovery scheme and QE detection. For the three lowest temperatures the values were also confirmed with the inversion recovery method. Seven to nine relaxation delays were collected. Time domain data were left-shifted to the echo maximum and processed with the 1 kHz exponential line broadening function. Magnetization build-up curves, corresponding to the integrated intensities of the full spectral regions, were fitted to a mono-exponential function.

The on resonance deuteron NMR rotating frame relaxation rates ($R_{1\rho}$) measurements[25] utilized the heat compensation scheme, with the spin-lock power of $\omega_{RF} = 20$ kHz and QE detection.[25] The off-resonance rotating frame relaxation ($R_{1\rho}^{off}$)measurements employed the adiabatic alignment of the magnetization with $\omega_{RF} = 30$ kHz. The adiabatic ramp had the modulations of form $\omega_{RF}(t) = \omega_{RF}\frac{\tanh\alpha(t/\tau)}{\tanh\alpha}$, $\Delta\Omega(t) = \Delta\Omega_0\frac{\tan((\text{atan}\beta)[1-t/\tau])}{\beta}$ for the RF field strength, and offset, respectively.[26] The relevant parameters were set to: the sweep $\Delta\Omega_0 = 120$ kHz, pulse duration $\tau = 200$ μs, and the steepness parameters $\alpha = 1.5$, $\beta = 5$. The values of offsets Ω ranged from 5 to 75 kHz. The interscan delay was set to 1.8 s for the spin-locking power of 20 kHz and 2.4 s for 30 kHz to minimize RF-induced heating. 10 to 12 relaxation delays were collected, with the maximum relaxation times not to exceed 35 ms to prevent RF-induced heating. 512 scans and 16 dummy scans were employed. The spin-locking field of $\omega_{RF} = 20$ kHz is sufficient for conducting the on-resonance $R_{1\rho}$ measurements because of significant narrowing of the line shapes in the 313 K to 242 K temperature range. The quality of spin-locking depends on the spectral frequencies and is demonstrated in Figure S10 for 313 K and 242 K temperatures. At 313 K all crystallites are locked within 90% and at 242 K over 80% of locking intensity is reached. It is also important to note that the modeling procedures for determination of motional parameters, briefly summarized in the next section, take into account the differential locking of crystallite orientation by explicitly modeling the coherent evolution during the spin-lock period.

Magnetization relaxation decay curves $M(t)$ were fitted to a mono-exponential function with a baseline of the form $M(t) = Ae^{-R_{1\rho}t} + B$. The integrated intensity of the entire powder pattern region was taken. Each individual crystallite orientation of the powder pattern in principle gives rise to a different relaxation rate.[25,62–63] In the presence of the distribution of the rate constant different approaches can be undertaken, such as taking the initial rate, analyzing the entire distribution of rates, assuming a bi-exponential form, or using the mono-exponential function with the baseline.[64–67] The latter approximation accounts for slowly relaxing components that are difficult to define precisely due to limitations on the maximum spin-lock time possible in the experiment. As long as the simulations procedure for motional modeling is performed using the relaxation delays that match the ones used in the experiment, this approximation will reliably define the faster end of the distribution that can be captured experimentally.[68]

The Q-CEST measurements utilized methodology previously described.[27] A weak RF field of 1.57 kHz was applied for 20 ms saturation time for a series of offsets between −60 to +60 kHz, followed by the QE detection scheme. 928 acquisition scans, 32 dummy scans, and the interscan delay of 0.9 s were employed. Spectra were processed with the 1 kHz exponential line broadening function. The CEST profiles consisted of integrated intensities of the whole powder pattern region.

The details of solid-state NMR measurements related to the determination of the M5 methyl group's ^{13}C chemical shift, conducted under the 60 kHz magic-angle spinning rate and at 14.1 T, are given in the legend to Figure S1. Solution NMR measurements for chemical shifts assignments have been performed at 11.7 T using a cryoprobe and the details are stated in SI1.

Modeling

The line shapes and laboratory frame T_1 relaxation rate were modeled with the EXPRESS program.[69] For the on and off resonance $R_{1\rho}$ simulations,[25] as well as those for the Q-CEST[27] the direct numerical integration of the full Liouville-von Neumann equation was performed.[28] The evolution during the spin-lock periods is governed by the quadrupolar coupling interactions for spin-1 deuterons.

The inter-conversion between the four symmetrical conformers of Figure 1B were modeled by the Markovian jumps between four sites with orientations fixed in the molecular frame. This approach is similar to what was employed previously for the Aβ fibrils and FMOC-methionine systems.[5,26] The rate constant of jumps between the sites, defined as the sum of the forward and backward rates, were assumed to be

the same between all pairs of sites. The occupation numbers for each of the sites, which we refer to as "weights", differed. The effect of fast methyl 3-site jumps was modeled through effective reduction in the value of quadrupolar coupling constant (C_q) by a factor of 3, with $C_q = 58$ kHz,[5] with the exception of simulations of T_1 times, for which they were included explicitly as an additional motional mode by nested frames.[69–70] The asymmetry parameter of the quadrupolar tensor was taken as zero.

The relaxation delays used in the simulations of the $R_{1\rho}$ and $R_{1\rho}^{off}$ rates matched the experimental ones. The effect of RF inhomogeneity was taken into account only for the Q-CEST simulations by including the 6-point grid of the inhomogeneity profile at 1.6 kHz, as described previously.[27,71] For the 20 and 30 kHz RF spin-lock amplitudes used in the rotating frame relaxation measurements, the inhomogeneity was very minor with the use of the Phoenix static probe[26] and, thus, was not included in the simulations.

Acknowledgements

This work was supported by the National Institutes of Health grants 1R15-GM111681 and S10OD011941, as well as by the NSF-MRI instrumentation grant CHE-1726947. Part of the measurements were performed at the National High Magnetic Field Laboratory, which is supported by NSF Cooperative Agreement NSF/DMR-1644779 and DMR-2128556, the State of Florida, and the U.S. Department of Energy.

Conflict of Interests

The authors declare no conflict of interest.

Data Availability Statement

The data that support the findings of this study are available from the corresponding author upon reasonable request.

Keywords: deuterium NMR · solid-state NMR · methionine · rotamers · low-complexity sequence

[1] N. D. Younan, R. C. Nadal, P. Davies, D. R. Brown, J. H. Viles, *J. Biol. Chem.* **2012**, *287*, 28263–28275.
[2] O. Carugo, *Biol. Chem.* **1999**, *380*, 495–498.
[3] Y. Miller, B. Ma, R. Nussinov, *J. Am. Chem. Soc.* **2011**, *133*, 2742–2748.
[4] A. Virrueta, C. S. O'Hern, L. Regan, *Proteins Struct. Funct. Genet.* **2016**, *84*, 900–911.
[5] L. Vugmeyster, M. A. Clark, B. I. Falconer, D. Ostrovsky, D. Gantz, W. Qiang, G. L. Hoatson, *J. Biol. Chem.* **2016**, *291*, 18484–18495.
[6] L. Vugmeyster, D. Ostrovsky, M. A. Clark, B. I. Falconer, G. L. Hoatson, W. Qiang, *Biophys. J.* **2016**, *111*, 2135–2148.
[7] L. Vugmeyster, D. Ostrovsky, *Chem. Phys. Lett.* **2017**, *673*, 108–112.
[8] T. A. Larsen, A. J. Olson, D. S. Goodsell, *Structure* **1998**, *6*, 421–427.
[9] S. Ovchinnikov, H. Kamisetty, D. Baker, *eLife* **2014**, *3*, e02030.
[10] F. Bumbak, M. Pons, A. Inoue, J. C. Paniagua, F. Yan, H. Wu, S. A. Robson, R. A. D. Bathgate, D. J. Scott, P. R. Gooley, J. J. Ziarek, *Cell Rep.* **2023**, *42*.
[11] A. B. Kleist, S. Jenjak, A. Sente, L. J. Laskowski, M. Szpakowska, M. M. Calkins, E. I. Anderson, L. M. McNally, R. Heukers, V. Bobkov, F. C. Peterson, M. A. Thomas, A. Chevigné, M. J. Smit, J. D. McCorvy, M. M. Babu, B. F. Volkman, *Science* **2022**, *377*, 222–228.
[12] G. L. Butterfoss, E. F. DeRose, S. A. Gabel, L. Perera, J. M. Krahn, G. A. Mueller, X. Zheng, R. E. London, *J. Biomol. NMR* **2010**, *48*, 31–47.
[13] K. T. O'Neil, W. F. DeGrado, *Trends Biochem. Sci.* **1990**, *15*, 59–64.
[14] T. I. Igumenova, K. K. Frederick, A. J. Wand, *Chem. Rev.* **2006**, *106*, 1672–1699.
[15] A. L. Lee, S. A. Kinnear, A. J. Wand, *Nat. Struct. Biol.* **2000**, *7*, 72–77.
[16] S. H. Gellman, *Biochemistry* **1991**, *30*, 6633–6636.
[17] R. L. Dunbrack, Jr., F. E. Cohen, *Protein Sci.* **1997**, *6*, 1661–1681.
[18] A. L. Lee, A. J. Wand, *Nature* **2001**, *411*, 501–504.
[19] L. Vugmeyster, D. Ostrovsky, M. Moses, J. J. Ford, A. S. Lipton, G. L. Hoatson, R. L. Vold, *J. Phys. Chem.* **2010**, *114*, 15799–15807.
[20] R. R. Vold, in *Nuclear Magnetic Resonance Probes of Molecular Dynamics* (Ed.: R. Tycko), Kluwer academic Publishers, Dordrecht, **1994**, pp. 27–112.
[21] M. J. Brown, R. L. Vold, G. L. Hoatson, *Solid State Nucl. Magn. Reson.* **1996**, *6*, 167–185.
[22] X. Shi, C. M. Rienstra, *J. Am. Chem. Soc.* **2016**, *138*, 4105–4119.
[23] Ü. Akbey, *J. Magn. Reson.* **2021**, *327*, 106974.
[24] L. Vugmeyster, D. Ostrovsky, *Prog. Nucl. Magn. Reson. Spectrosc.* **2017**, *101*, 1–17.
[25] L. Vugmeyster, D. Ostrovsky, *ChemPhysChem* **2019**, *20*, 333–342.
[26] L. Vugmeyster, A. Rodgers, D. Ostrovsky, C. James McKnight, R. Fu, *J. Magn. Reson.* **2023**, *352*, 107493.
[27] L. Vugmeyster, D. Ostrovsky, R. Fu, *ChemPhysChem* **2020**, *21*, 220–231.
[28] L. Vugmeyster, *Solid State Nucl. Magn. Reson.* **2021**, *111*, 101710.
[29] M. McDonald, H. Box, W. Bian, A. Kendall, R. Tycko, G. Stubbs, *J. Mol. Biol.* **2012**, *423*, 454–461.
[30] A. T. Petkova, R. D. Leapman, Z. H. Guo, W. M. Yau, M. P. Mattson, R. Tycko, *Science* **2005**, *307*, 262–265.
[31] A. K. Paravastu, R. D. Leapman, W. M. Yau, R. Tycko, *Proc. Natl. Acad. Sci. USA* **2008**, *105*, 18349–18354.
[32] A. C. Murthy, G. L. Dignon, Y. Kan, G. H. Zerze, S. H. Parekh, J. Mittal, N. L. Fawzi, *Nat. Struct. Mol. Biol.* **2019**, *26*, 637–648.
[33] A. C. Murthy, N. L. Fawzi, *J. Biol. Chem.* **2020**, *295*, 2375–2384.
[34] Y. K. Al-Hilaly, C. Hurt, J. E. Rickard, C. R. Harrington, J. M. D. Storey, C. M. Wischik, L. C. Serpell, A. B. Siemer, *Front. Neurol. Neurosci.* **2022**, *16*, 988074.
[35] M. D. Tuttle, G. Comellas, A. J. Nieuwkoop, D. J. Covell, D. A. Berthold, K. D. Kloepper, J. M. Courtney, J. K. Kim, A. M. Barclay, A. Kendall, W. Wan, G. Stubbs, C. D. Schwieters, V. M. Y. Lee, J. M. George, C. M. Rienstra, *Nat. Struct. Mol. Biol.* **2016**, *23*, 409–415.
[36] S. Khodadadi, A. P. Sokolov, *Soft Matter* **2015**, *11*, 4984–4998.
[37] L. Hong, N. Smolin, B. Lindner, A. P. Sokolov, J. C. Smith, *Phys. Rev. Lett.* **2011**, *107*.
[38] H. Jansson, R. Bergman, J. Swenson, *J. Phys. Chem. B* **2011**, *115*, 4099–4109.
[39] W. Doster, *J. Non-Cryst. Solids* **2011**, *357*, 622–628.
[40] J. Kraus, S. Sarkar, C. M. Quinn, T. Polenova, in *Annual Reports in NMR Spectroscopy, Vol. 102* (Ed.: G. A. Webb), Academic Press, **2021**, pp. 81–151.
[41] K. Wüthrich, G. Wider, G. Wagner, W. Braun, *J. Mol. Biol.* **1982**, *155*, 311–319.
[42] R. Richarz, K. Wüthrich, *Biopolymers* **1978**, *17*, 2133–2141.
[43] S. Schwarzinger, G. J. Kroon, T. R. Foss, P. E. Wright, H. J. Dyson, *J. Biomol. NMR* **2000**, *18*, 43–48.
[44] P. Schanda, *J. Magn. Reson.* **2019**, *306*, 180–186.
[45] P. Rovó, *Solid State Nucl. Magn. Reson.* **2020**, 101665.
[46] L. S. Batchelder, C. E. Sullivan, L. W. Jelinski, D. A. Torchia, *Proc. Natl. Acad. Sci. USA* **1982**, *79*, 386–389.
[47] T. H. Huang, R. P. Skarjune, R. J. Wittebort, R. G. Griffin, E. Oldfield, *J. Am. Chem. Soc.* **1980**, *102*, 7377–7379.
[48] M. V. Shapovalov, R. L. Dunbrack, Jr., *Structure* **2011**, *19*, 844–858.
[49] Y. Xue, M. S. Pavlova, Y. E. Ryabov, B. Reif, N. R. Skrynnikov, *J. Am. Chem. Soc.* **2007**, *129*, 6827–6838.
[50] W. Doster, *Eur. Biophys. J.* **2008**, *37*, 591–602.
[51] L. Vugmeyster, D. Ostrovsky, A. Khadjinova, J. Ellden, G. L. Hoatson, R. L. Vold, *Biochemistry* **2011**, *50*, 10637–10646.
[52] L. Vugmeyster, D. Ostrovsky, J. J. Ford, A. S. Lipton, *J. Am. Chem. Soc.* **2010**, *132*, 4038–4039.
[53] A. G. Palmer, 3rd, *J. Magn. Reson.* **2014**, *241*, 3–17.

[54] L. Vugmeyster, D. Fai Au, M. C. Smith, D. Ostrovsky, *ChemPhysChem* **2021**, *23*, e202100709.
[55] L. Vugmeyster, D. Osrovsky, T. R. Villafranca, J. Sharp, W. Xu, A. S. Lipton, G. L. Hoatson, R. L. Vold, *J. Phys. Chem. B.* **2015**, *119*, 14892–14904.
[56] W. Doster, S. Cusack, W. Petry, *Nature* **1989**, *337*, 754–756.
[57] V. Réat, R. Dunn, M. Ferrand, J. L. Finney, R. M. Daniel, J. C. Smith, *Proc. Natl. Acad. Sci. USA* **2000**, *97*, 9961–9966.
[58] S. Khodadadi, J. E. Curtis, A. P. Sokolov, *J. Phys. Chem. B* **2011**, *115*, 6222–6226.
[59] S. Khodadadi, S. Pawlus, J. H. Roh, V. G. Sakai, E. Mamontov, A. P. Sokolov, *J. Chem. Phys.* **2008**, *128*, 5.
[60] W. Doster, *Physica B+C* **2006**, *385–86*, 831–834.
[61] J. R. Lewandowski, M. E. Halse, M. Blackledge, L. Emsley, *Science* **2015**, *348*, 578–581.
[62] R. L. Vold, R. R. Vold, in *Advances in Magnetic and Optical Resonance, Vol. 16* (Ed. W. Warren), Acadenic Press, San Diego, **1991**, pp. 85–171.
[63] J. R. C. van der Maarel, *J Chem Phys* **1993**, *99*, 5646–5653.
[64] P. A. Beckmann, E. Schneider, *J. Chem. Phys.* **2012**, *136*, 054508.
[65] W. Schnauss, F. Fujara, K. Hartmann, H. Sillescu, *Chem. Phys. Lett.* **1990**, *166*, 381–384.
[66] B. Geil, G. Hinze, *Chem. Phys. Lett.* **1993**, *216*, 51–55.
[67] R. H. A. Kohlrausch, *Ann. Phys.* **1854**, *167*, 179–214.
[68] L. Vugmeyster, D. F. Au, D. Ostrovsky, R. Fu, *ChemPhysChem* **2019**, *20*, 1680.
[69] R. L. Vold, G. L. Hoatson, *J. Magn. Reson.* **2009**, *198*, 57–72.
[70] L. Vugmeyster, D. Ostrovsky, *Methods* **2018**, *148*, 136–145.
[71] L. Vugmeyster, D. Ostrovsky, A. Greenwood, R. Fu, *Front. Mol. Biosci.* **2021**, *8*.

Manuscript received: August 9, 2023
Revised manuscript received: December 1, 2023
Version of record online: January 4, 2024